Ionization in intense laser fields beyond the electric dipole approximation: concepts, methods, achievements and future directions

Journal Article

Author(s):
Maurer, Jochen; Keller, Ursula (iD)

Ionization in intense laser fields beyond the electric dipole approximation: concepts, methods, achievements and future directions

J Maurer[ID] **and U Keller**[*][ID]

Department of Physics, ETH Zurich, 8093 Zurich, Switzerland

E-mail: jocmaure@phys.ethz.ch and keller@phys.ethz.ch

CrossMark

Abstract

The electric dipole approximation is widely used in atomic, molecular and optical physics and is typically related to a regime for which the wavelength is much larger than the atomic structure. However, studies have shown that in strong laser fields another regime exists where the dipole approximation breaks down. During the ionization process in intense laser fields and at long wavelengths the photoelectrons can reach higher velocities such that the magnetic field component of the laser field becomes significant. The ionization dynamics and the final momentum of the electron is therefore modified by the entire Lorentz force. In contrast the magnetic field interaction is neglected in the dipole approximation. Rapid developments in laser technology and advancements in the accuracy of the measurements techniques have enabled the observation of the influence of such non-dipole effects on the final angular photoelectron momentum distributions. More recently the number of studies on ionization beyond the dipole approximation has increased significantly, providing more important insight into fundamental properties of ionization processes. For example we have shown that the final three dimensional photoelectron momentum spectra is significantly affected by the non-dipole drift with the parent–ion interaction, the linear multiphoton momentum transfer on a sub-cycle time scale and the sharing of the transferred linear photon momenta between the electron and the ion. In this article we present an overview of the underlying mechanisms and we review the experimental techniques and the achievements in this field. We focus on ionization in strong laser fields in the regime where the dipole approximation is not valid but a fully relativistic description is not required.

Keywords: strong-field ionization, atomic, molecular and optical physics, non-dipole effects

(Some figures may appear in colour only in the online journal)

---

[*] Author to whom any correspondence should be addressed.

1. Introduction

When an atom is exposed to a light field with either a photon energy larger than the ionization potential or a sufficiently intense laser pulse, the atom can become ionized and at least one electron is released from the atom. The laser field transfers energy, angular momentum and linear photon momentum to the outgoing electron which is also referred to as the photoelectron. To facilitate the description of the ionization process, the electric dipole approximation has been widely used in atomic, molecular and optical physics, ranging from single photon transitions to strong-field ionization. Within this approximation, a light field is approximated by a spatially homogeneous electric field and vector potential (i.e. $\vec{A}(\vec{r}, t) \equiv \vec{A}(t)$) neglecting the magnetic field interaction because $\vec{B}(t) = \nabla \times \vec{A}(t) = 0$ [1]. Whereas the transfer of energy from the laser field to the electron is captured within the dipole approximation, the transfer of linear photon momentum or the influence of the magnetic laser field component is not.

With the widespread use of Ti:sapphire laser amplifier systems, the majority of strong-field experiments have been performed at around 800 nm, a wavelength that typically supports the dipole approximation [2]. In this wavelength regime both the size of an atomic or even molecular target is small compared to the wavelength and the magnetic field interaction can be neglected at moderate intensities. Therefore for most strong-field experiments in the near-infrared (near-IR) around 800 nm and intensities of up to 10^{14} W cm^{-2}, the dipole approximation is justified within the typical measurement accuracy.

However, by moving either to higher intensities [3, 4] or to longer wavelengths [5, 6], the dipole approximation is not fulfilled anymore and significant changes can be observed in photoelectron angular distributions and photoelectron momentum distributions (PMD). The first experimental observation of the influence of the magnetic laser field component in strong-field ionization measurements were reported at very high intensities on the order of 10^{18} W cm^{-2} in multiple ionization of noble gases [3, 4]. First measurements at a longer 3.4 μm wavelength in the mid-infrared (mid-IR) regime [5, 7, 8] showed that the dipole approximation breaks down already at moderate intensities on the order of 5×10^{13} W cm^{-2}.

This scaling of the strength of non-dipole effect with a longer wavelength might appear counter-intuitive at a first glance, in particular since the momentum of one photon scales with the inverse wavelength. However by increasing the wavelength the maximal kinetic energy reaches higher values and the electron in the laser field starts to be affected by the interaction with the magnetic component of the laser field [5, 6].

Both in single photon ionization and in strong-field ionization, it is very well understood how the energy is transferred to the electron. However, there have been some open questions regarding the transfer of linear momentum of the involved photons to the photoelectron. Recent studies provided some fundamental aspects of the ionization beyond the dipole approximation which initially may have appeared to be counter-intuitive. In particular, the final photoelectron momenta in strong-field ionization showed significant differences for linear polarization and small ellipticities due to the rescattering dynamics with the parent ion driven by the entire Lorentz force [5, 7, 9, 10]. For example in this regime the maximum of the photoelectron distribution is shifted opposite to the laser beam propagation direction, what appears to be counter-intuitive within the framework of the radiation pressure brought forward in earlier work with circular polarization [11]. Not only the final momentum is significantly affected by rescattering of the returning electron wavepackets with the parent ion. In addition we have observed a time delay between the ionization phase with maximum ionization probability and the ionization phase with the smallest linear photon momentum transfer [8]. Additional insight concerns the momentum sharing between the electron and the ion in both single photon and strong-field ionization. These recent results may have an impact on potential future experiments with regards to the time-dependent linear photon-momentum transfer and the attosecond timing can potentially be used as a probe to better understand light-induced ultrafast processes [8, 12]. Furthermore these results have implications on the usage of the popular length gauge and the widely used tunnel ionization picture [6].

To date review articles on this topic have focussed mainly either on the fully relativistic regime or on photoionization in general [13]. The strong-field ionization was treated briefly with various theoretical methods to describe strong field ionization beyond the dipole approximation [14]. Further topical reviews exist for the fully relativistic case at extremely high intensities, again with the focus on theory, see e.g. reference [15]. Here we provide a review on the non-dipole effects that are caused by interaction of the magnetic laser field component in strong field ionization with the focus on experiments and their underlying fundamental understanding at moderate intensities with negligible relativistic contributions. This regime is interesting because the parent–ion interaction plays a significant role and novel measurement techniques give access to the transferred photon momentum as a function of the attosecond ionization time delays. We discuss the timing of linear photon momentum transfer and its impact of the non-dipole effects using the attoclock measurement technique with the goal to access the timing of the tunnel ionization process. We also briefly discuss some studies of single photon ionization and the case of relativistic strong-field ionization to place our research on this topic into a broader context.

The article is organized as follows: in section 2 we introduce the electric dipole approximation, in section 3 we discuss the various criteria for the limits of the dipole approximation reported in literature, in sections 4 and 5 the experimental and theoretical methods. In sections 6, 8 and 7 we present the achievements in the field so far and in section 9 we discuss possible future directions in this field. We conclude the article with some remarks in section 10.

J. Phys. B: At. Mol. Opt. Phys. **54** (2021) 094001

J Maurer and U Keller

2. The vector potential, the scalar potential and the electric dipole approximation

2.1. The potentials and the fields

The most common way to define the electric dipole approximation is via an expansion of the vector potential of the light field (atomic units are used throughout the text unless indicated otherwise).

Let us first have a look at the vector potential itself. The vector potential $\vec{A}(\vec{r}, t)$ is a vector field that determines the measurable quantities of interest of a light wave, the electric field vector $\vec{E}(\vec{r}, t)$ and the magnetic field vector $\vec{B}(\vec{r}, t)$. The electric field component is connected to the vector potential via the time derivative:

$$\vec{E}(\vec{r}, t) = -\frac{\partial \vec{A}(\vec{r}, t)}{\partial t}. \quad (1)$$

In the presence of an additional scalar potential $\Phi(\vec{r}, t)$, the electric field is modified by adding $-\nabla\Phi(\vec{r}, t)$ to the total electric field. The magnetic field component of the light field is obtained by the rotation of the vector field [16]:

$$\vec{B}(\vec{r}, t) = \nabla \times \vec{A}(\vec{r}, t). \quad (2)$$

As a consequence of the Maxwell-equations and the relations above, the vector potential satisfies the homogeneous wave equation:

$$\nabla^2 \vec{A}(\vec{r}, t) - \frac{1}{c^2}\frac{\partial^2 \vec{A}(\vec{r}, t)}{\partial t^2} = 0. \quad (3)$$

The wave equation has plane waves and superpositions of such as solutions and their corresponding vector potential is described as follows:

$$\begin{aligned}\vec{A}(\vec{r}, t) &= \vec{A}_0 \exp\left(i(\vec{k} \cdot \vec{r} - \omega t)\right) \\ &= \vec{A}_0 \exp\left(i\vec{k} \cdot \vec{r}\right) \exp\left(-i\omega t\right).\end{aligned} \quad (4)$$

The electric dipole approximation is essentially the leading order approximation of the expansion of the exponential function [17]:

$$\exp\left(i\vec{k} \cdot \vec{r}\right) = 1 + i\vec{k} \cdot \vec{r} + \cdots \approx 1. \quad (5)$$

That means that argument of the oscillating exponential function is approximated as $\vec{k} \cdot \vec{r} - \omega t \approx -\omega t$. The spatial dependence vanishes and the vector potential depends solely on the time. Since the fields are in general related to the vector potential via $\vec{E}(\vec{r}, t) = -\frac{\partial \vec{A}(\vec{r}, t)}{\partial t}$ and $\vec{B}(\vec{r}, t) = \nabla \times \vec{A}(\vec{r}, t)$, the corresponding electric field is spatially homogeneous as well [17]:

$$\vec{E}(t) = -\frac{\partial \vec{A}(t)}{\partial t}. \quad (6)$$

The electric field is thus described as a spatially homogeneous vector field that oscillates in time. The field does not have any spatial dependence or structure and does not travel in any direction like a real light wave. A travelling wave cannot be represented within the dipole approximation.

As a further consequence, any interaction with magnetic field component of the laser field is neglected in the dipole approximation:

$$\vec{B} = \nabla \times \vec{A} = 0. \quad (7)$$

2.2. Gauges and corresponding Hamiltonians

In general, the potentials $\Phi(\vec{r}, t)$ and $\vec{A}(\vec{r}, t)$ are not uniquely defined by the fields. Gauge transformations of the form

$$\vec{A}(\vec{r}, t) \rightarrow \vec{A}'(\vec{r}, t) = \vec{A}(\vec{r}, t) + \nabla\chi \quad (8)$$

$$\phi \rightarrow \phi' = \phi - \frac{\partial \chi}{\partial t} \quad (9)$$

leave the fields $\vec{E}, \vec{B}$ unaltered. Thus, the interaction of light with matter can be described in any gauge resulting from a gauge transformation as described by equations (8) and (9).

In general, a single atomic electron system in a light field characterized by the vector potential $\vec{A}(\vec{r}, t)$ and an electric field characterized by the scalar potential ϕ can be described by the following Hamiltonian, regardless of the gauge:

$$H = \frac{\vec{p}^2}{2} - \frac{1}{2}\left(\vec{A}(\vec{r}, t) \cdot \vec{p} + \vec{p} \cdot \vec{A}(\vec{r}, t)\right) + \frac{\vec{A}^2(\vec{r}, t)}{2} - \phi. \quad (10)$$

For a hydrogen-like atom with charge Z, the scalar potential is $\phi = \frac{Z}{r}$. The corresponding time-dependent Schrödinger equation (TDSE) describing the atomic single electron system reads:

$$i\hbar\frac{\partial}{\partial t}\psi(\vec{r}, t) = H\psi(\vec{r}, t). \quad (11)$$

The most notable gauges in strong-field physics beyond the dipole approximation are the Lorentz-gauge and the Coulomb gauge [18]. In the Lorentz-gauge, the potentials satisfy the so-called Lorentz-condition $\nabla \cdot \vec{A}(\vec{r}, t) + \frac{1}{c^2}\frac{\partial \phi}{\partial t} = 0$ whereas in the Coulomb-gauge the vector potential satisfies the condition $\nabla \cdot \vec{A}(\vec{r}, t) = 0$ [18]. Thus, the Coulomb-gauge Hamiltonian reads:

$$H_{\text{Coulomb}} = \frac{\vec{p}^2}{2} - \vec{A}(\vec{r}, t) \cdot \vec{p} + \frac{\vec{A}^2(\vec{r}, t)}{2} - \phi. \quad (12)$$

The Coulomb-gauge is sometimes called radiation gauge, although in some cases authors refer to the name radiation gauge only for the case when no sources are present and $\phi = 0$ [18]. The radiation-gauge Hamiltonian reads:

$$H_{\text{Rad}} = \frac{\vec{p}^2}{2} - \vec{A}(\vec{r}, t) \cdot \vec{p} + \frac{\vec{A}^2(\vec{r}, t)}{2}. \quad (13)$$

In the case when the dipole approximation is applied and $\vec{A}(\vec{r}, t) = \vec{A}(t)$, the corresponding gauge with the condition $\nabla \cdot \vec{A}(t) = 0$ is called velocity gauge [18].

$$H_{\text{Velocity}} = \frac{\vec{p}^2}{2} - \vec{A}(t) \cdot \vec{p} + \frac{A^2(t)}{2} - \phi. \quad (14)$$

It should be noted that the velocity gauge offers the additional simplification that a suitable gauge transformation of

J. Phys. B: At. Mol. Opt. Phys. **54** (2021) 094001

J Maurer and U Keller

the *wave function* allows for the elimination of the $A(t)^2$-term. This simplification is possible in the dipole approximation, because the A^2 contribution causes only a time-dependent phase modulation of the wave function.

Within the dipole approximation, an additional gauge is frequently applied, the length gauge. The length gauge or Göppert-Mayer-gauge [19] is obtained by the transformation function of the form $\chi = -\vec{r} \cdot \vec{A}(t)$ based on the initial potentials $\phi = 0$ and $\vec{A} \approx \vec{A}(t)$. The resulting vector potential in the length gauge is zero and the scalar potential is $\phi = -\vec{r} \cdot \vec{E}(t)$. This means that the light field as well as the whole light–matter interaction is described by a scalar potential, a fundamental difference to the velocity gauge.

The length gauge Hamiltonian in the dipole approximation then becomes:

$$H_{\text{Length}} = \frac{\vec{p}^2}{2} - \vec{E}(t) \cdot \vec{r} - \phi. \tag{15}$$

Within the dipole approximation, the length gauge is ubiquitous in strong-field physics. In particular it is the basis for the widely used tunnel ionization model. However, the validity of its usage for travelling light fields including strong laser fields was questioned [6, 20, 21].

In fully relativistic strong-field physics there is a relativistic version of the Göppert-Mayer-gauge that employs four vector potentials that allows a description of travelling waves—however only in the fully relativistic description beyond the dipole approximation [18]. Whereas the name length gauge does only refer to the gauge within the dipole approximation, the name Göppert-Mayer-gauge can refer to both, the dipole case or the fully relativistic case.

A common method to approximately describe the non-dipole interaction is based on [22]

$$\vec{A}(\vec{r}, t) \approx \vec{A}(t) + (\vec{r} \cdot \nabla) \vec{A}(\vec{r}, t) \Big|_{\vec{r}=0} = \vec{A}(t) + \frac{\hat{k} \cdot \vec{r}}{c} \vec{E}(t), \tag{16}$$

where $\hat{k}$ denotes the unity vector in direction of the laser propagation.

Inserting this approximation into the Hamiltonian and neglecting terms $\propto \frac{1}{c^2}$ leads the to following Coulomb-gauge Hamiltonian [22]:

$$H_{\text{approx}}(\vec{r}, t) = \frac{\vec{p}^2}{2} + \vec{A}(t) \cdot \vec{p} + \frac{\vec{A}^2(t)}{2} + \frac{\hat{k} \cdot \vec{r}}{c} \left(\vec{p} + \vec{A} \right) \cdot \vec{E}(t). \tag{17}$$

In addition, there are more gauges used to describe light–matter interaction, such as for example the propagation gauge [23, 24]. However, they have rarely been used in the description of strong-field ionization at parameters discussed in this article.

3. Limits of the validity of the electric dipole approximation

The electric dipole approximation breaks down when the wavelength of the laser field approaches the size of the atomic structure. In this case the explicit spatial dependence of the field and the vector potential needs to be taken into account. In strong laser fields, the electric dipole approximation breaks down not only for such short wavelengths but also in the long-wavelength regime. In this case, the influence of the magnetic field becomes significant as the velocity of the photoelectron increases with increasing wavelength at a fixed intensity. In this section, we present various criteria to estimate the parameter space for which the dipole approximation breaks down. The criteria rely on characteristics of the dynamics of an unbound electron in a laser field and we consider this situation first.

We would like to point out that the criteria discussed below should only be considered as a rough guideline for the electric dipole approximation. In principle, in a travelling wave the spatial dependence of the vector potential and the related forces along the beam propagation direction are always present. Ultimately the sensitivity of the measurement determines the limits of the dipole approximation.

3.1. Dynamics of an unbound electron in a laser field

The dynamics of an unbound electron in a laser field is an important concept for strong-field physics. For a first rough approximation the influence of the parent–ion interaction is neglected and the photoelectron can be considered as an unbound electron in a laser field after it is released from the bound atomic state. The dynamics of a free electron in an intense laser field with a kinetic energy significantly exceeding the photon energy can be described by classical fields. In this case the Volkov state is an exact solution to the Schrödinger equation of one electron in a classical electromagnetic plane wave [25]. A Volkov state is composed of plane waves that are modulated by the vector potential [18]:

$$\Psi_{\text{Volkov}} = \exp \left(i\vec{p} \cdot \vec{r} - i\frac{p^2}{2}t - i\int_{-\infty}^{t} H_I(p, \tau)\mathrm{d}\tau \right), \tag{18}$$

where $H_I = \vec{A} \cdot \vec{p} + \vec{A}^2$ denotes the interaction Hamiltonian.

The concept then can be further simplified when we also treat the electron with a classical model. The motion of a classical electron in a classical strong laser field is the basis for the continuum dynamics of the electron in the widely used two-step model of strong-field ionization [26, 27]. The classical electron dynamics beyond the dipole approximation differs fundamentally in one point from the dynamics within the dipole approximation. Within the dipole approximation, the field does only exert forces onto the electron along the direction of the electric field in linear polarization or within the polarization plane for elliptical polarization. Thus there is no force component acting onto the electron perpendicular to the polarization plane along the laser beam propagation direction. When we go beyond the dipole approximation this is not the case anymore and the magnetic field component causes forces and momentum transfer to the photoelectron along the beam propagation direction. In the frame of reference where the electron is on average at rest, the influence of the magnetic field component of the laser field leads to a characteristic figure-eight motion in linear polarization [6, 21, 28]. The
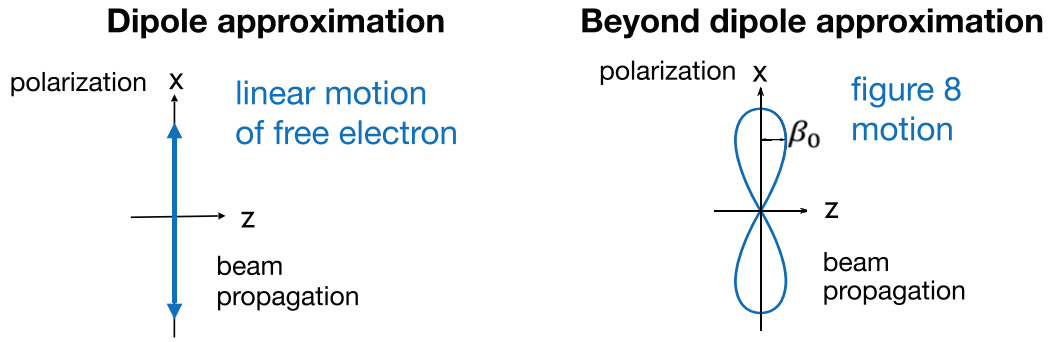
Dipole approximation

polarization x

linear motion
of free electron

z

beam
propagation

Beyond dipole approximation

polarization x

β_0

figure 8
motion

z

beam
propagation

Figure 1. Illustration of the classical dynamics of an unbound electron within and beyond the dipole approximation for the case of linear polarization. Within the dipole approximation, the electron describes a linear motion in the laser field. By moving beyond the dipole approximation, there is a force component perpendicular to the electric field polarization direction. In the frame of reference where the drift velocity of the electron in laser beam propagation direction (i.e. the forward drift) is zero, it describes the characteristic figure-eight-motion with an amplitude β_0 along the laser propagation direction.
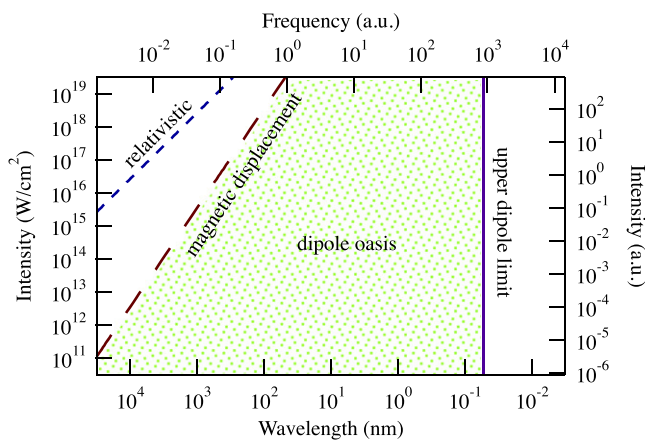
Figure 2. Illustration of the validity range of the dipole approximation. The dipole approximation is considered as valid according to [21] in the green-dotted area of the parameter space [5].

figure-eight motion and respective dynamics within the dipole approximation are illustrated in figure 1.

3.2. Amplitude of figure-eight-motion

Various criteria for the limits of the validity of the electric dipole approximation have been introduced. We present three commonly used criteria, they all focus on the drift of the electron wave packet within an optical cycle. First, we consider the figure-eight motion of a free electron in a laser field in the frame of reference where in the frame of reference where the drift velocity of the electron in laser beam propagation direction (i.e. the forward drift) is zero. When the amplitude of the figure-eight motion along the laser beam propagation direction approaches 1 atomic unit, non-dipole effects need to be taken into account (figure 2) [6, 21]. This quantity is characterized by

$$\beta_0 \approx \frac{U_\text{p}}{2mc\omega}. \tag{19}$$

The lower limit for the validity of the dipole approximation is thus given by the condition

$$\beta_0 \approx 1 \text{ a.u.} \tag{20}$$

with the corresponding condition for the limiting intensity

$$I_\text{limit} = 8c\omega^3. \tag{21}$$

3.3. Magnitude of forward-drift

A complementary approach to the amplitude of the figure-eight motion introduced in the preceding subsection is to estimate the magnitude of the forward drift that is induced onto the electron per laser cycle in the laboratory frame. This drift per cycle can be expressed as [29, 30]:

$$\chi_0 = \frac{\pi e^2 E_0^2}{2m^2 c\omega^3}. \tag{22}$$

When this drift per cycle approaches one 1 a.u., non-dipole-effects need to taken into account.

3.4. Lorentz deflection parameter

In strong laser fields with low elliptical polarization the liberated electron wavepacket can be driven back to the parent ion and rescatter. One way to characterize the influence of the laser magnetic field onto the rescattering electron dynamics is the Lorentz deflection parameter [31–33]:

$$\Gamma_\text{R} = \left(\frac{p_\text{zd}}{\Delta_\perp}\right)^2 = \gamma \frac{U_\text{p}^2}{\omega c^2}. \tag{23}$$

The Lorentz deflection parameter is a measure of the ratio of the average drift momentum $p_\text{zd} = \frac{U_\text{p}}{c}$ and the width $\Delta_\perp = \frac{\sqrt{E_0}}{(2I_\text{p})^{-1/4}}$ of the released electron wave packet. U_p denotes the ponderomotive potential of the electron, I_p the ionization potential of the target and γ the Keldysh parameter [34]. According to this criterium, when $\Gamma_\text{R} > 1$, non-dipole contributions need to be taken into account in the rescattering dynamics.

3.5. Fully relativistic dynamics vs non-dipole behaviour

When the ponderomotive potential $U_\text{p} = \frac{I}{4\omega^2}$ of the electron in the laser field approaches its rest energy mc^2 we are not only well beyond the dipole approximation but the dynamics also

become relativistic [22]. It was suggested to use the intensity parameter $z_f = \frac{2U_p}{mc^2}$ to quantify the onset of fully relativistic behaviour via the condition $z_f = 1$ [6]. Note that the appearance of the magnetic field component in a light field is rooted in relativistic electrodynamics [16]. The onset of the influence of the magnetic field component starts to become significant at non-relativistic intensities when it comes to the interaction of an electron with a light field.

As an example, the drift that is induced per cycle by the magnetic field onto a free electron in a laser field is about 10 a.u. in a field with a wavelength of 800 nm and an intensity of 9×10^{15} W cm^{-2} whereas the ratio of $\frac{U_p}{mc^2}$ does not approach unity unless we move to intensities as high as 9×10^{18} W cm^{-2} [22].

4. Experimental methods

4.1. Requirements to the instrumentation

Non-dipole features can in principle be observed in the photoelectron energy spectrum. However, the energy spectrum is a rather insensitive probe for non-dipole effects because they induce mainly a reduction of the absolute height of the spectrum related to a change in the ionization rate [35]. In contrast, under the same conditions a significant alteration of the photoelectron angular distribution can be observed [35]. In particular, the influence onto the angular distribution can be observed without any reference except the knowledge of the polarization plane of the laser beam propagation direction. The same argument holds for non-dipole effects on 2D and 3D momentum distributions. In case the zero momentum along the beam propagation direction is known, the non-dipole effects can be observed as asymmetries and shift along the laser beam propagation direction.

Thus, the main requirement for the observation of non-dipole effects in photoelectron distributions is a suitable detector with angular momentum resolution. Ideally a three dimensional (3D) momentum distribution of the photoelectrons should be measured. In addition, the electron spectrometer needs to have a sufficiently high resolution to observe the non-dipole effects. Typically the spectrometer needs to be able to image electrons with an energies on the order of $\gtrsim 50$ eV with a required resolution of about $\frac{\Delta p}{p} \approx 0.01$.

Experiments to probe non-dipole effects greatly benefit from a sufficiently high accuracy of the momentum zero. So far, two methods have been reported for an accurate calibration of the zero momentum in strong-field ionization. One method exploits a sharp spot in the PMD that is created by the ionization of atoms that are left in highly excited states by the laser pulse and are subsequently ionized by the spectrometer field [5, 7, 8, 10, 11, 33]. Another method is to use photoelectron spectra from counterpropagating laser beams. In this case, the magnetic field component is cancelled and the resulting PMD is expected to be symmetric around the zero momentum plane [36].

4.2. Suitable photoelectron spectrometers

4.2.1. VMI spectrometer. One experimental method to observe non-dipole effects in strong-field ionization is a velocity map imaging (VMI) spectrometer [37, 38] which was used for several investigations [5, 7, 8, 10, 11]. In its traditional form, it consists of three electrostatic plates that form an electrostatic lens focussing charged particles onto a position-sensitive detector, usually a microchannel plate.

A VMI spectrometer records directly a two-dimensional PMD. The resolution for photoelectrons of a VMI spectrometer is typically on the order of $\frac{\Delta p}{p} \approx 0.01$. The traditional three-plate arrangement can typically limit the maximal electron energies with a maximum electron momenta of 2–2.5 a.u.. However, this limitation can be overcome with thick-lens designs [39].

Another limitation of VMI setups is the restriction to two-dimensional projections of the full 3D PMD. This limitation can be overcome by the application of tomographic reconstruction schemes. Tomographic reconstruction schemes have already been successfully applied in various experiments with VMI spectrometers within [40–43] and beyond the dipole approximation [5, 7, 8, 10, 11].

4.2.2. COLTRIMS/reaction microscope. Another widely used apparatus to record momentum distributions of charged particles are cold target recoil ion momentum spectroscopy (COLTRIMS), sometimes also referred to as reaction microscope [44, 45]. The main characteristic of the COLTRIMS detector is the capability to record electrons and ions of fragmentation processes in coincidence.

COLTRIMS detectors have been recently successfully used to measure non-dipole effects in strong-field ionization [36, 46] and in single-photon ionization [47]. The latter work is of particular interest as the first experimental work that directly measures the linear photon momentum transferred to both the photoelectron and the ion in coincidence.

4.3. Suitable light sources

Most of the amplified femtosecond laser sources were based on the Ti:sapphire laser technology and the vast majority of strong-field experiments have been performed at wavelengths of around 800 nm. Typical peak intensities for single ionization are on the order of 10^{14} W cm^{-2}. In this regime, the dipole approximation is still valid and non-dipole effects are considered as not significant. However, in the case of sufficiently high intensities and high momentum resolution, non-dipole effects can still be measured even in this near-IR regime [36].

Early works [3, 4] were performed with a Nd:YLF chirped-pulse amplification (CPA) system that delivered pulses with 1 ps duration at a centre wavelength of 1053 nm with an energy of several hundreds of mJ per pulse, however with the trade-off of a very low repetition rate of one shot per 70 s.

More suitable laser source for ionization experiments operate at mid-IR wavelengths. In particular, all measurements on

this topic in our group were performed with an optical parametric CPA-source that operates at a centre wavelength of 3.5 μm [48, 49]. More laser sources with high repetition rates are being developed, allowing for more exciting experiments in this direction [50].

So far, experiments on single photon ionization that were sensitive to the linear photon momentum have been performed at synchrotron sources [47, 51–53].

5. Theoretical methods

5.1. Unbound electron in a laser field

The dynamics of an unbound classical electron without any additional potentials or forces in a laser field is well understood. When the influence of the parent–ion interaction is neglected, an analytical solution is given for the final momentum of the photoelectron that appears at an initial phase η_0 with an initial momentum $\vec{p}_0$ in the pulse, including all relativistic effects [28, 54]:

$$\vec{p}_\mathrm{f} = \vec{p}_0 - \vec{A}(\eta_0) + \hat{\vec{z}}\left(\frac{1}{2\beta}\,\vec{A}(\eta_0)\cdot(\vec{A}(\eta_0) - 2\,\vec{p}_{0,\perp})\right) \quad (24)$$

with $\beta = \frac{E_0}{c} - p_{0,z}$ and $E_0 = \sqrt{p_0^2 + c^4}$.

From equation (24) follows with $\beta \approx c$ that an electron initially at rest and with a final kinetic energy E_f has a momentum along the beam propagation axis of $p_{z,\mathrm{f}} = \frac{E_\mathrm{f}}{c}$.

5.2. Tunnel ionization, two-step model and CTMC methods

The widely used two-step model of strong-field ionization uses quantum mechanical tunnel ionization theory as the first step and a fully classical model without any parent–ion interaction as a second step [26, 27, 55, 56]. In the initial tunnelling step, the Coulomb-potential $-1/R$ is superimposed by the laser field with the length gauge potential $-x \cdot E$, where the laser electric field is directed along the x-direction perpendicular to the laser beam propagation z. The resulting potential creates a tunnelling barrier, where the electron can tunnel into a classically allowed region. In the classically allowed region, the classical electron dynamics is described by the Newton equation of motions which normally also neglects the parent–ion interaction. The two-step model of strong field ionization can be used as a basis for classical trajectory Monte Carlo (CTMC) methods. By sampling the initial momentum space according to the initial conditions provided by tunnel ionization theory, an ensemble of electrons is created that resembles the electron wavepacket. The electron wave packet is propagated fully classically. When the parent–ion interaction is included, the propagation needs to be solved numerically, unless the Coulomb potential is treated perturbatively [7, 8, 57]. Another aspect of the inclusion of the parent–ion interaction is that the initial position of the electron is a significant contribution to the final momentum.

The initial positions and momenta of the electrons can be deducted from the adiabatic tunnel ionization theory [55] or non-adiabatic tunnel ionization theory [56, 58–61]. It should

be noted that the results from reference [55] are contained in references [56, 58–60] as a special case, see e.g. [62, 63].

The key differences between the two limiting cases for the adiabatic and non-adiabatic theory are the different initial positions at the exit of the tunnel and the inclusion of an initial momenta along the rotation direction of the electric field in case of elliptical or circular polarization [61]. At near-IR wavelengths the non-adiabatic effects have shown to play a significant role for the final electron momenta [64]. However, they play only a minor role at mid-IR wavelengths [65]. More sophisticated models for the initial momentum, initial positions and for the propagation in the field include the influence of the induced dipole due to the polarizability of the atom and the ion as well as the usage of a parabolic coordinate system for the initial step [66, 67].

For dynamics beyond the dipole approximation, one might question the initial conditions based on a calculation in the dipole approximation. Although the method proved to be successful to explain the experimental results [5, 7, 8] and effects beyond the dipole approximation onto bound states are expected to be minor, modifications might be needed to fully account for non-dipole effects even on the initial wave packet [8, 68].

There have been theoretical attempts to include relativistic and non-dipole effects in trajectory-based models in the initial tunnel ionization step [69, 70]. The models predict that the non-dipole effects on the sub-barrier dynamics lead to a change in ionization probability as well as a small initial momentum at the moment when the electron appears in the continuum.

Purely classical models of the electron propagation in the laser field cannot reproduce any interference effects. This issue can be overcome by weighting each electron trajectory with the phase $\exp(iS)$, where S is the action of the electron trajectory. In combination with CTMC methods and initial conditions from the adiabatic approximation, this approach is referred to as quantum trajectory Monte Carlo (QTMC) model [10, 71].

5.3. Strong-field approximation

The strong-field approximation (SFA) is a method to obtain an approximate solution of the Schrödinger equation for the case of strong-field ionization. The idea behind is an approximation how to calculate the transition rate between the initial state and a Volkov state, i.e. the quantum-mechanical state of an unbound electron in a laser field [34, 72, 73]. The SFA does not include the influence of the parent–ion interaction for direct ionization, but can be included for rescattering.

One of the more serious issues with the SFA is that generally not the same result is obtained for the length and the velocity gauge. The gauge independence is only achieved for an initial s-state.

Relativistic and non-dipole versions of the SFA have been reported [22, 35, 68, 74–78]. A common approach to facilitate the calculation is the approximation of the spatial integral in the transition amplitude with the saddle-point approximation [68, 75]. This approximation comes however with the loss of information about the influence of the initial state.

The saddle-point approximation is the basis for the transition to semiclassical models such as for example the Coulomb-corrected SFA [79]. A successful implementation of this approach beyond the dipole approximation was reported in references [10, 80].

5.4. Time-dependent Schrödinger equation

The most exact theoretical approach using classical fields is the numerical solution of the TDSE. In contrast to the SFA, the solution of the TDSE leads to the same result independent of the chosen gauge and with all Coulomb-effects included. What is not included in TDSE calculations are photon fluctuations and photonic effects in general and any effect of the target onto the laser field itself.

For the vast majority of the reported results the TDSE was solved within the dipole approximation. However, there have been successful efforts to solve the TDSE beyond the dipole approximation. The main drawback of the TDSE-approach is the high demand of computational resources and therefore focal volume effects that require the calculation for a whole set of intensities, are typically not considered in TDSE-calculations.

The high demand of computational resources is even more challenging in the parameter space where the dipole approximation breaks down, i.e. at high intensities and long wavelengths. In that case the large oscillation amplitudes of the electron wave packet require large box sizes for the calculation, whereas the Coulomb potential still dictates the required resolution in the positions space.

Solutions of the TDSE beyond the dipole approximation have been reported in references [22, 29, 36, 68, 81–87].

5.5. Photon picture of strong-field ionization

So far there have been only few theoretical approaches reported that provide a full quantum mechanical treatment of both the atom and the laser field [88, 89]. The approach might not be applicable in a straightforward manner to calculate energy spectra and momentum distributions and is rather of theoretical interest to place strong-field physics in a quantum electrodynamical framework. However, the photon picture is a powerful tool when it comes to the application of momentum and energy conservation arguments to understand energy and momentum spectra. A notable example of this is the interpretation of the peak structure occurring in above-threshold ionization in terms of the absorption of multiple photons [90]. In this case, the final drift kinetic energy of an electron ionized from a target with ionization potential I_p by N photons is:

$$E_f = N\hbar\omega - I_p - U_p. \tag{25}$$

Conservation of momentum requires that both the angular momentum and the linear momentum of the photons involved in the ionization process needs to be transferred to the electron–ion system.
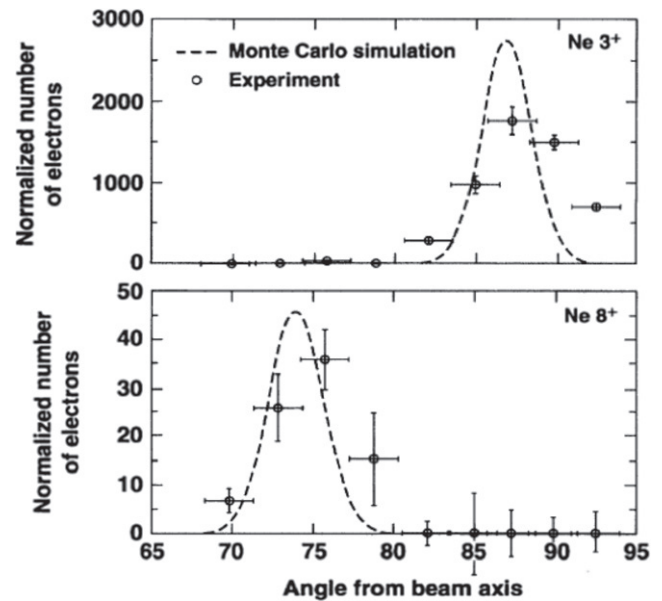

Figure 3. Photoelectron angular distributions from multiple ionization of neon by strong-field ionization of noble gases with circularly polarized 1 ps laser pulses at a centre wavelength of 1053 nm. The angular distributions for both presented species, Ne^{3+} and Ne^{8+} show clear deviations from the expected angle of 90 degree. The results were reasonably well reproduced by classical Monte-Carlo simulations (dotted line). Reprinted figure with permission from [3], Copyright (1995) by the American Physical Society.

6. Direct strong-field ionization with circular and elliptical polarization

6.1. Effect on final cycle-averaged photoelectron momentum

Let us first consider the case of direct ionization of the target. In this case, the electron is ionized from the target atom without rescattering during the ionization process.

Pioneering work on strong-field ionization beyond the dipole approximation was reported in reference [3, 4], where authors presented the angular distribution from multiple ionization of noble gases at comparably high intensities on the order of 10^{18} W cm^{-2}. The results were obtained with 1 ps pulses at a centre wavelength of 1053 nm (figure 3). The angular distributions show a clear deviation from the 90-degree angle towards the laser beam propagation direction that one would expect within the dipole approximation (figure 3). Furthermore, the authors report a relationship between the kinetic energies of the electrons and the deviation angle: The higher the ionization number of the atom, the higher is the kinetic energy of the electron and in turn the angle deviation along the beam propagation direction. The results are in good agreement with CTMC simulations (the dotted line in figure 3). The comparison of non-relativistic and fully relativistic calculations showed that under their experimental conditions, the effect of the relativistic mass shift needed to be included.

The influence of the radiation pressure was observed with circular polarization in a work by Smeenk *et al*. The work
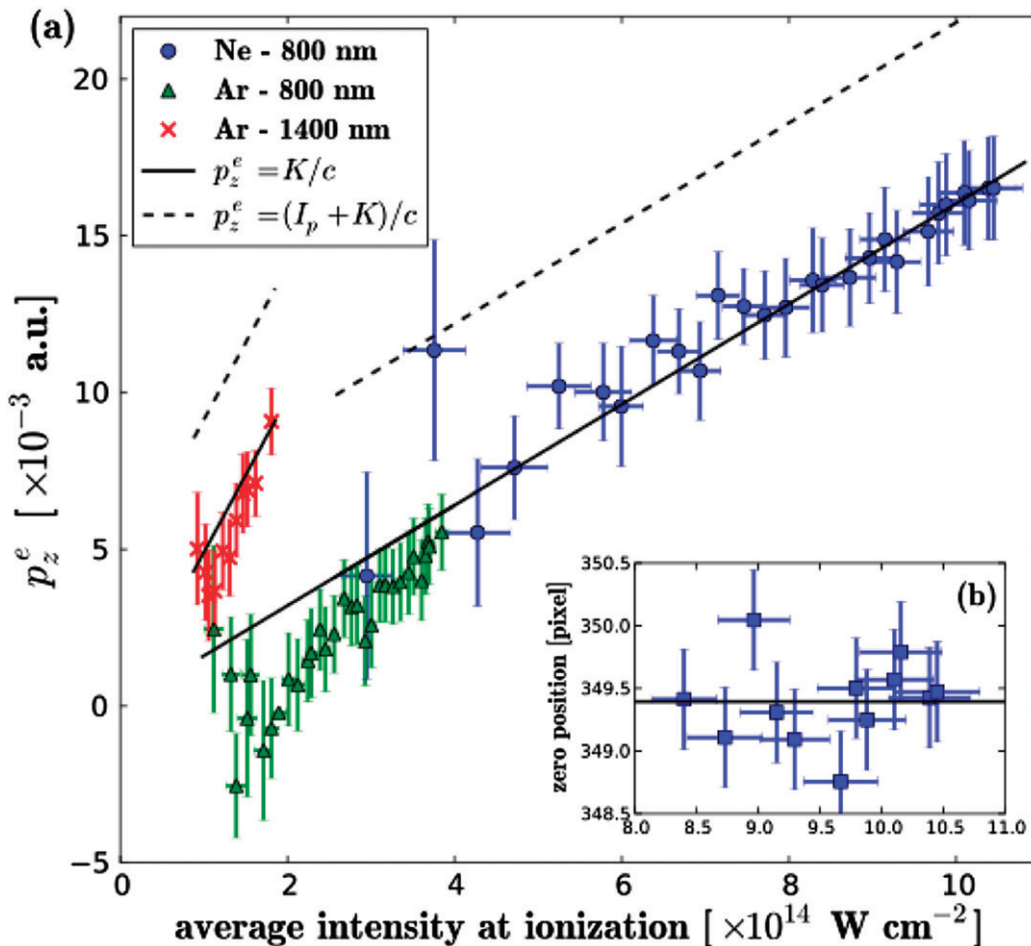
Figure 4. Shift along the beam propagation direction of PMDs from strong field ionization with circular polarization. The PMDs are shifted along the beam propagation direction. Reprinted figure with permission from [11], Copyright (2011) by the American Physical Society. The authors explained the shift with a radiation pressure model.

was performed with circularly polarized pulses at two different wavelengths, at 800 nm and 1400 nm, with the two noble gas targets argon and neon at intensities ranging from 0.15–1×10^{15} W cm^{-2} [11]. The data were recorded with a VMI spectrometer and the authors analysed the expectation value of the projected momentum distribution along the beam propagation direction (figure 4). The results were interpreted in terms of a radiation pressure picture. The main conclusions of the article can be summarized as follows: (i) there is a measurable shift of the PMD in the laser beam propagation in measurements with circularly polarized pulses. (ii) The shift can mostly be explained within the error bars by the momentum that was transferred during the continuum propagation of the electron.

Interestingly, the data for low intensities showed a significant discrepancy from the radiation pressure model. After the publication of the work by Smeenk *et al*, a theoretical article used a Coulomb-scattering wave function to describe their results and to provide first indication for the influence of parent–ion interaction at low intensities [78].

In addition, the authors point out with a simple model calculation that in measurements with linear polarization, the expectation value of the transferred momentum is expected to be significantly smaller than in the circularly polarized case due

to the variation of the highly nonlinear ionization rate during the pulse. The ionization rate maximizes at phases when the momentum transfer in beam propagation minimizes.

6.2. Effect on final photoelectron momentum as a function of the ionization phase

Most investigations on non-dipole effects in direct strong-field ionization focus on the cycle-averaged final photoelectron momentum. To date only few studies have been published on the linear photon momentum transfer as a function of the ionization phase, i.e. the phase when the electron was released to the continuum.

One experimental work from Willenberg *et al* [8] studied the linear photon momentum transfer as a function of the ionization phase (figure 5). The authors concluded that the transferred final linear momentum depends on the phase of ionization within a cycle. With the attoclock principle, the connection between the streaking angle of a photoelectron and the time or phase of ionization within the optical cycle can be made [91–93]. Counterintuitively, the minimum of the transferred linear multi-photon momentum occurred for the electron trajectory that were ionized approximately at a phase where the ionization rate maximizes. In principle this behaviour can be
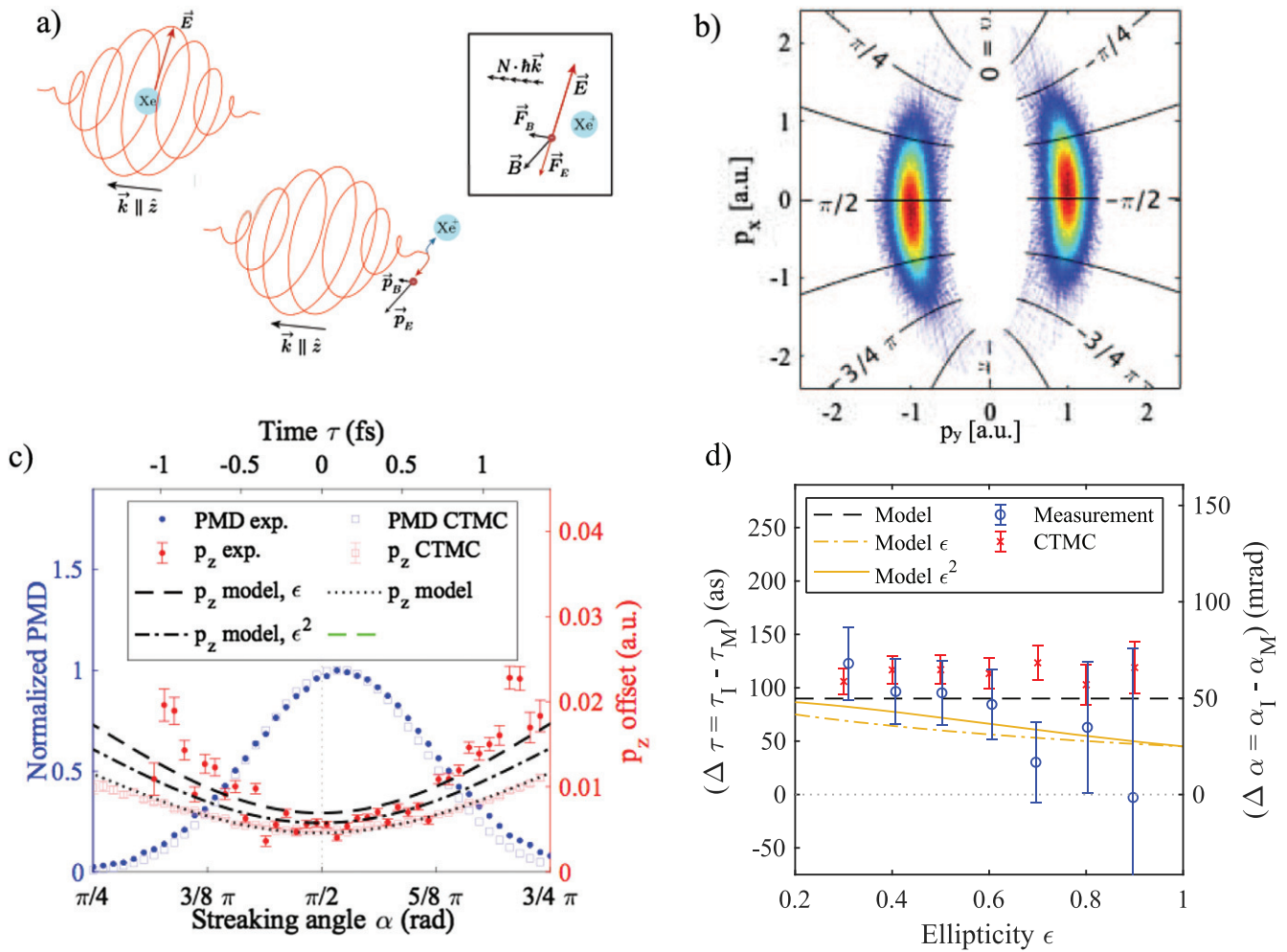
Figure 5. (a) Illustration of the measurement principle. The electron is getting ionized and is subsequently streaked in the laser field. The transferred momentum in the polarization plane and the transferred momentum along the laser propagation z depends on the time of ionization that, in turn, is imprinted on the streaking angle [8]. (b) Polarization plane PMD with elliptical coordinates. Elliptical coordinates allow for a linear mapping of time to streaking angle even with ellipticities significantly smaller than $\epsilon \approx 1$ [8]. (c) Ionization yield and the p_z-shift as a function of the ionization time. The measurement shows a clear offset in the ionization phase between the minimal p_z-shift and the maximal ionization yield. This offset translate to a time delay between the most probable electron trajectory and the one with minimal momentum transfer. In addition to the results from CTMC calculations, we show the curves from the pure classical propagation ('model') and from two models with an ellipticity-dependent initial momentum along the beam propagation axis ('model ϵ', 'model ϵ^2') [8]. (d) Difference in streaking angle of the most probable electron trajectory (α_I) and the one with minimal momentum transfer (α_M) and corresponding time delay $\Delta\tau$ as function of the ellipticity together with the corresponding results from the CTMC-calculation and the analytical models [8].

explained by the phase shift between the electric field, that dictates the ionization rate and the vector potential that dictates the final momentum of the electron. The final momentum of an electron ionized at a phase η_0 with initial momentum zero follows $\propto \frac{A_0^2}{c}$ [54].

However, having a closer look, the ionization phases of the minimal momentum transfer and the maximal ionization rate do not exactly coincide (figure 5). The difference of the streaking angle translates to a time difference in the sub-cycle ionization phases with the attoclock principle. The authors observed a time-delay that was induced by the Coulomb-potential on the order of 100 as. In more detail, the classical electron continuum trajectory that leads to the minimal transferred linear momentum starts with a negative delay with respect to the most likely electron continuum trajectory, i.e. the ones that ends at the final momentum where the ionization rate maximizes.

This means that the electron trajectory with the minimal linear momentum transfer is advanced with respect to the one with the highest ionization probability. The experiment suggests that a phase- and ellipticity-dependent correction might be needed to fully understand the data (figure 5).

So far, there is only one study on the theory of the sub-cycle linear multiphoton momentum transfer that was published very recently [68]. The authors present numerical solutions of the sub-cycle resolved momentum shift along the beam propagation direction with SFA and TDSE calculations alongside with analytical solutions. Similar to the results of the experimental work in reference [8], they find a minimum in the momentum transfer along the minor axis of the polarization ellipse with an additional dependence on the carrier envelope phase. Furthermore, they found a sub-cycle dependence of the initial electron momentum that is attributed to the coupling of non-adiabatic effects with the linear photon
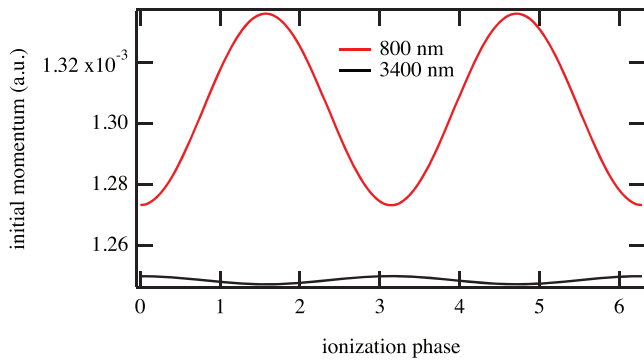
Figure 6. The initial momentum in beam propagation direction as a function of the ionization phase for 800 nm and 3400 nm at an intensity of $1 \cdot 10^{14}$ W cm^{-2} and an ellipticity of $\epsilon = 0.8$ caused by the non-adiabatic coupling with non-dipole effects according to equation (S34) of reference [68]. The variation over the ionization phase is significantly smaller for 3400 nm than for 800 nm, indicating that this influence of the non-adiabatic coupling with non-dipole effects plays only a minor role in the mid-IR.

Figure 7. Photoelectron angular distributions represented as surfaces of photoionization in the high-intensity, high-frequency non-dipole regime (from reference [94]) for five-cycle pulse with $\omega = 2$a.u. and field strengths of 20 a.u., 30 a.u. and 45 a.u.. The laser propagation direction is marked with an arrow. On the left the calculation within the dipole approximation and on the right side the full non-dipole calculation. Beyond the dipole approximation, the familiar two-lobe structure evolves into a three-lobe structure due to the parent–ion interaction. Reprinted figure with permission from [94], Copyright (2011) by the American Physical Society.

momentum transfer. An estimate according to equation (S34) of reference [68] suggests that the non-dipole drift due to the non-adiabatic coupling is significantly smaller for 3400 nm than for 800 nm (figure 6).

7. Rescattering in strong-field ionization influenced by non-dipole effects

7.1. Linear polarization

Most studies on non-dipole effects in strong laser fields have had their focus on direct ionization. Early theoretical studies with linear polarization that included rescattering with the parent ion focussed on extremely high intensities on the order of 10^{19} W cm^{-2} and very short wavelengths of few tens of nanometers [82, 83, 94, 95]. Whereas in references [82, 83] the authors observed the forward drift due to the magnetic field component in snapshots of their TDSE-simulation at different times, no final distributions after the pulse where provided. In references [94, 95] Førre *et al* reported that in their parameter range the photoelectron angular distribution changes from the characteristic two-lobe structure that is expected within the dipole approximation to a three-lobe structure (figure 7) and showed that the underlying dynamics can be explained classically. They could separate the interplay between the non-dipole forces from the laser field and the parent–ion interaction.

At mid-IR wavelengths, the first experimental study on the interplay of the Coulomb field and the magnetic field component of the laser field was reference [5]. The authors studied various noble gases and recorded projections of the PMD with a VMI spectrometer. The target was ionized by mid-IR few-cycle laser pulses with the polarization axis parallel to the detector plane with intensities ranging from 0.5–1×10^{14} W cm^{-2}, a parameter range where the dipole approximation starts to break down. Ludwig *et al* identified the peak of the PMD by fitting the projection of the PMD onto the beam propagation axis. The main observation was that the
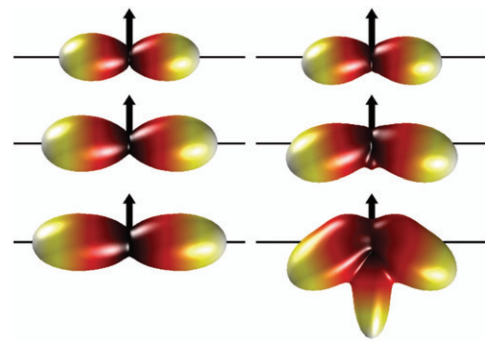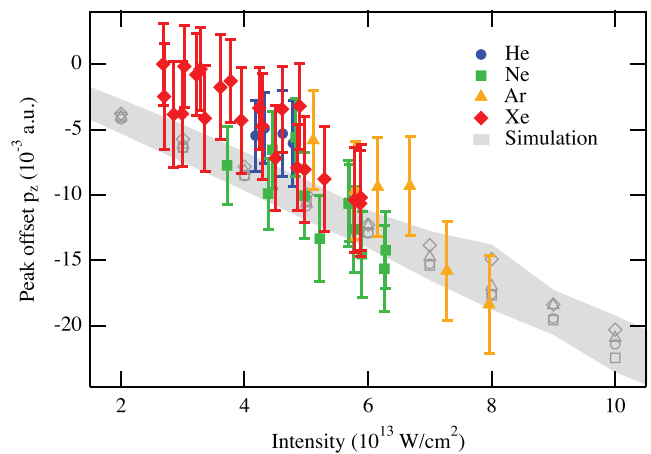

Figure 8. Offset of the peak of the PMD projected onto the beam propagation axis z for a wavelength of 3.4 μm [5]. The peaks are shifted opposite to the beam propagation direction and the negative offset increases with increasing intensity [5].

peak of the PMD was shifted opposite to the beam propagation direction (figure 8), which was at a first glance a counterintuitive behaviour. The puzzle was solved with numerical simulation to study the interplay between the forces from the laser field and the parent–ion interaction. Using CTMC simulations that include both the parent–ion field and the magnetic field component of the laser field could explain the experimental result. The interplay between the Coulomb force and the magnetic field component of the laser field explained the initially surprising behaviour. An intuitive picture can be given as follows. The Lorentz force pushes the electron initially along the beam propagation direction. Upon return to the parent ion with an offset along the beam propagation direction, the parent–ion Coulomb interaction slingshots the electron opposite to the beam propagation direction.

A similar behaviour was reported [46] from measurements in argon in the intensity range 0.5–1.5×10^{15} W cm^{-2} at
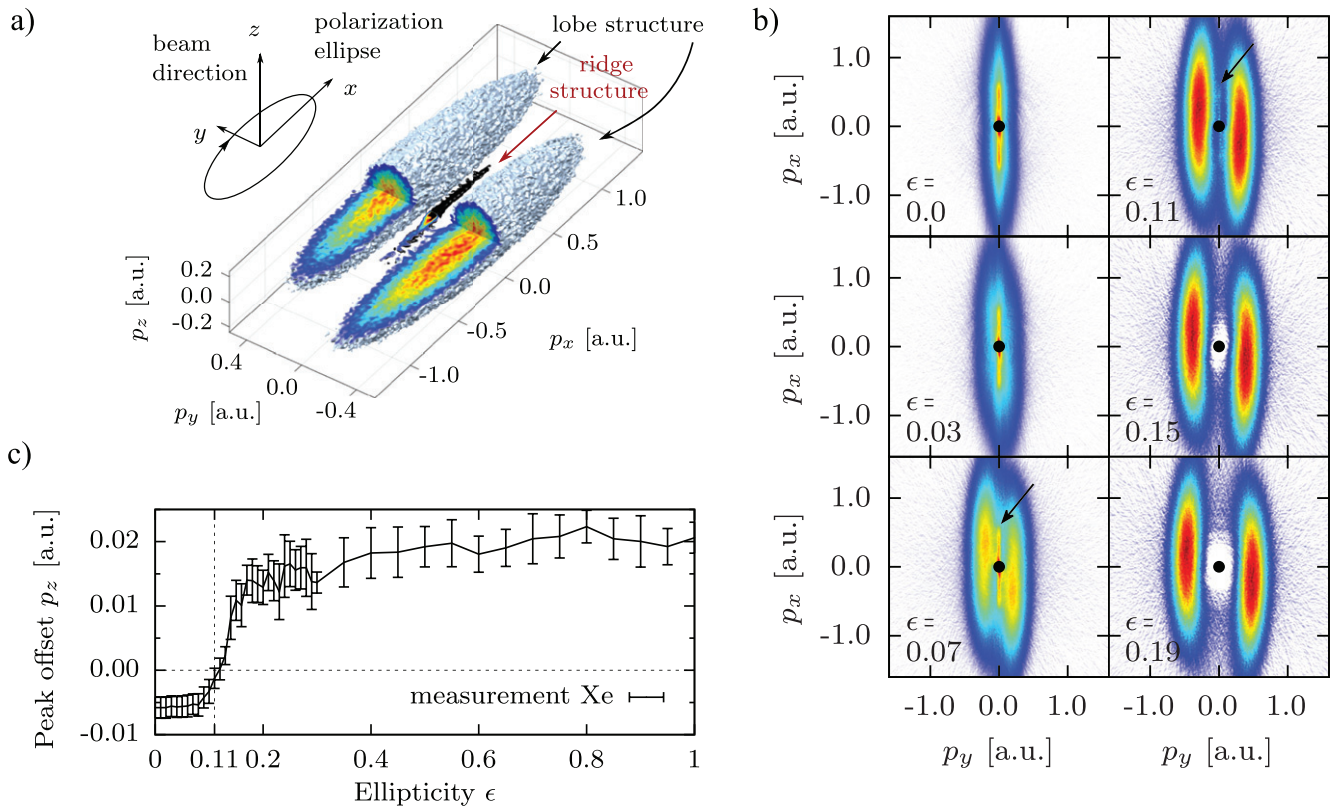
Figure 9. (a) Isosurface of a reconstructed PMD recorded at a wavelength of 3.4 μm and an intensity of 6×10^{13} W cm^{-2} with elliptical polarization ($\epsilon = 0.11$). The PMD shows the lobes due to direct electrons and the ridge that stems from Coulomb-focused electrons. (b) Polarization plane cuts of the 3D PMDs. The ridge (marked with black arrows) vanishes with increasing ellipticity. (c) The peak of the PMD as a function of the ellipticity. The peaks transitions with increasing ellipticity from negative values (opposite to the beam propagation direction) to positive values (along the beam propagation direction) of p_z. Reprinted figure with permission from [7], Copyright (2018) by the American Physical Society.

800 nm, leading to a momentum offset opposite to the beam propagation direction of up to 1.3×10^{-2} a.u.. The results were reproduced with a relativistic *ab initio* calculation [46]. Semiclassical calculations regarding the effect on both, the photoelectron and the ion, are discussed in reference [96].

In linear polarization, a small fraction of the electrons can undergo a process called high-order above-threshold ionization. The photoelectrons from this process undergo backward scattering that can lead to photoelectrons with a high kinetic energy that exceeds the energy cutoff of $2U_p$ expected from direct electrons and electrons that undergo only forward scattering during the strong-field ionization process. Theoretical studies on the influence of the non-dipole effects on high-order above-threshold ionization were reported in references [85, 86].

7.2. Elliptical polarization

At small ellipticities, the electron may not necessarily rescatter in the sense that the centre part of the electron wavepacket hits the parent ion, but it still may be affected when it returns to the proximity of the ion. In the work of Maurer *et al* [7], the authors used this characteristic to shed more light on this behaviour. They recorded projected PMDs under similar experimental conditions as in reference [5], scanning the elliptical polarization of the laser pulse from

linear to close-to-circular. The peak of the PMD was identified in analogy to reference [5]. The analysis revealed that the peak of the PMD transitions from negative p_z-values (opposite to the beam propagation direction) to positive p_z-values (along the beam propagation direction) when the ellipticity is increased (figure 9). The crossover was observed at an ellipticity of $\epsilon \approx 0.12$.

Moreover, the authors recorded full 3D PMDs of for small ellipticities close to the one where the turnover occurs ($\epsilon = 0, 0.03, 0.07, 0.11, 0.15, 0.19$) to gain further insight. The full 3D PMDs revealed a remarkable feature that is connected to the ellipticity-dependence of the position of the peak along the beam propagation momentum axis. The authors observed a sharp ridge that is only apparent at small ellipticities ($\epsilon < 0.12$).

Having a closer look at the ridge, the authors realized that the ridge projected onto the momentum axis of laser beam propagation peaks at momentum opposite to the beam propagation direction. Under the experimental conditions of reference [7], the ridge is essentially separated from the lobes formed by the direct electrons (indicated in figure 9), allowing for a separate analysis of the Coulomb-focussed and the direct electrons. This showed for the PMD projections along beam propagation axis that the ridge peak is shifted in opposite direction and the lobe peaks with the direct electrons are shifted along the beam propagation direction. The observations lead
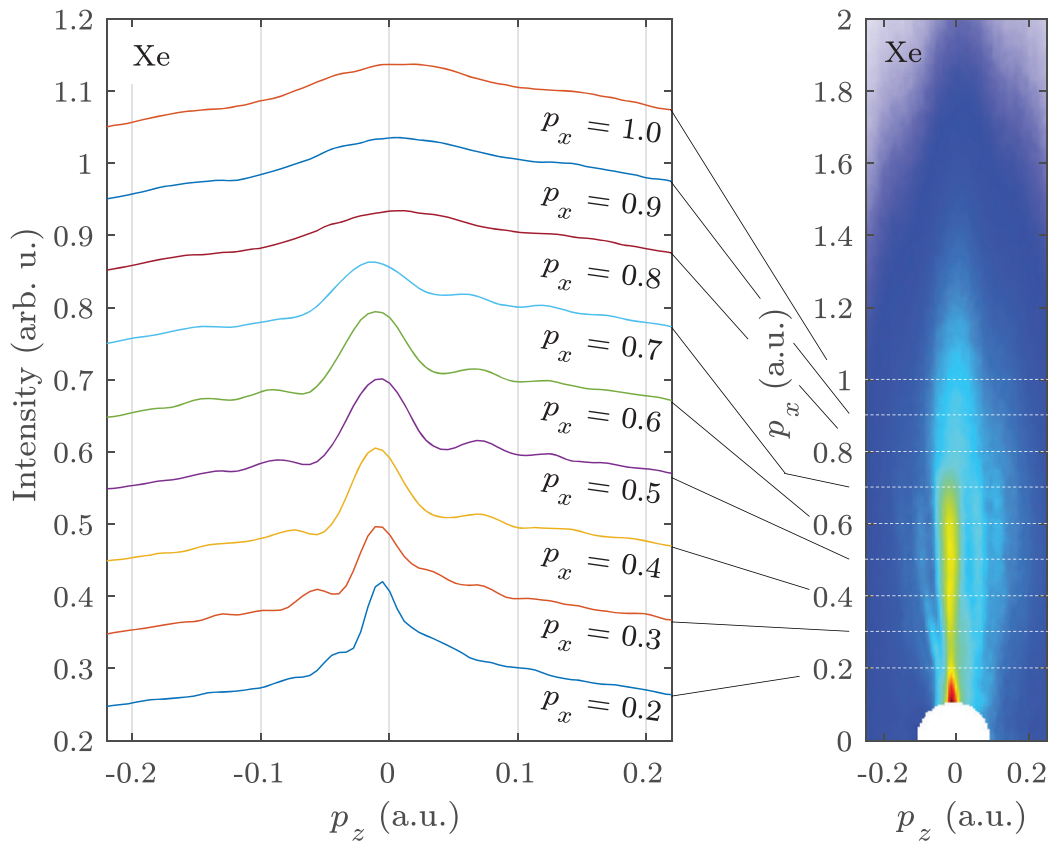
Figure 10. PMD (*right panel*) recorded from xenon at a wavelength of 3.4 μm and an intensity of 7×10^{13} W cm^{-2}, together with lineouts (*left panel*) at various values of p_x. The linear polarization vector was along the *x*-direction. The figure exhibits the clear asymmetry of the holographic fringes [10].

to the conclusion that peaks of the PMD at linear polarization and at low ellipticities are caused by the ridge structure and are present as long as the ridge dominates over the lobes of the direct electrons. At higher ellipticities, the ridge vanishes, the lobes of direct electrons start to dominate and the projected PMD peaks a values along the beam propagation direction. The unique analysis relying on the momentum space separation of the direct and Coulomb-focussed electrons of reference [7] was only possible under experimental condition in the mid-IR, where the dipole approximation breaks down at intensities where single ionization is dominant and the influence of the Coulomb-potential is significant.

7.3. Holographic interferences in strong-field ionization

In strong-field ionization with linear polarization one can observe various kinds of interferences in the final momentum distributions. One type of interference that can occur in strong-field ionization are intra-cycle interferences between an electron trajectory that rescatters significantly with the parent ion and an electron trajectory that is barely influenced by the parent–ion potential (i.e. a direct electron), both trajectories ending up at the same final momentum [79, 97]. Due to the conceptual similarity to information storage in an holographic image, that contains the interference information from a direct wave and one diffracted by the object, this type of interference in the PMD is called holographic interferences. One

can also observe non-dipole effects in the holographic interferences of the PMD because both the direct and rescattering photoelectron trajectories are affected by the magnetic field component of the laser. Non-dipole effects in holographic interference structures have been observed in experiments [10] and theory [10, 98, 99]. Experimental results of the holographic interference pattern are shown in figure 10, where the asymmetry of the holographic fringes is clearly visible. The experimental results of [10] could be largely explained with semiclassical simulations and the influence of the focal volume onto the interferences was observed and explained with QTMC-simulations. Another conclusion of reference [10] is the coincidence of the ridge discovered in reference [7] with the central interference lobe of the holographic interference pattern.

7.4. Nonsequential strong-field double ionization

Double ionization is a common process in strong-field ionization, in particular at high intensities [100]. For linear [101] and elliptical polarization [102, 103], the first electron can ionize a second electron upon recollision with the ion. Both electrons experience the influence of the magnetic field component of the laser and alter the electron trajectories during the ionization process. Strong-field double ionization beyond the dipole approximation was studied in experiment [104] and theory [104–106]. One of the findings was that the sum of the

momenta photoelectrons exceed the average of the photoelectron momentum along the beam propagation direction by an order of magnitude. Strong recollisions were pinpointed as a cause for this unexpected behaviour [105].

7.5. High-order harmonic generation

High-order harmonic generation (HHG) is a process based on the recollision of the electron with the parent ion, leading to the emission of photons with frequencies of multiple times the frequency of the driving laser field. The upper limit or cut-off energy of the emitted photons is determined by the $I_p + 3.17U_p$, where I_p denotes the ionization potential of the target and U_p the ponderomotive energy [27]. There has been an ongoing interest to move from near-IR to longer wavelengths for the driving laser with the goal to create photons with higher energy and obtain table-top high-flux XUV and x-ray sources [50]. However, just as in the strong field ionization processes that serve as the basis for HHG, the mid-IR wavelengths will introduce effects beyond the dipole approximation [107]. During the ionization process the magnetic field component of the driving laser can cause a drift of the wavepacket along the beam propagation axis with the consequence that the centre part misses the parent ion leading a reduction of the HHG yield [22, 108, 109]. Another observable influence onto the HHG spectrum, according to theory, is the occurrence of odd and even order harmonics as the dynamical symmetry is broken by the magnetic field component of the laser field. Within the dipole approximation, one would expect the occurrence of only odd harmonics [110, 111].

8. Momentum sharing between the electron and the ion

Momentum conservation in physics requires that all the linear photon momentum that is absorbed from the field is transferred to the ionization fragments.

In general, for a single ionization process where in total N photons are absorbed by the target that is initially at rest we obtain:

$$N\hbar\vec{k} = \vec{p}_{ion} + \vec{p}_{electron}. \tag{26}$$

When we assume $\vec{k}\|\hat{z}$, the momentum conservation for the z-component reads:

$$N\hbar k_z = p_{ion,z} + p_{electron,z} \tag{27}$$

However, the question, how the linear photon momenta $N\hbar\vec{k}$ is distributed between the ion and the electron, is not trivial and is different in single photon and multi-photon/strong-field ionization. We would like to point out that the parent ion does not necessarily need to remain in the ground state after the ionization.

8.1. Single photon ionization

In single photon ionization, nearly the full linear photon momentum can be transferred to the outgoing electron. Earliest predictions of the momentum sharing in photoionization were done by Sommerfeld where the photoelectron distribution was shifted by nearly twice the expected value from the transferred momentum of the photon [112]. This would, in turn, lead to a momentum of the ion opposite to the direction of the incoming photon. The fraction F of the linear photon that is transferred to the electron can be calculated from the photoelectron angular distribution $J(\theta, \phi)$ via $F = \frac{\int mv \cos\theta J \, d\Omega}{\int (h\nu/c)J \, d\Omega}$. Calculations for an 1s-state of the momentum fraction given to the electron have as result $F = \frac{8}{5}K$, $K = \frac{1/2mv^2}{h\nu} = \frac{h\nu - I_p}{h\nu}$ [112–114]. For initial states other than 1s-orbitals, this value fraction can differ drastically [115]. We would like to point out that there is surprisingly little experimental data available on momentum sharing in single photon ionization, despite the first predictions on this topic are already nearly 90 years old [112].

The first measurements of the momenta of the electron and the ion were only recently published [47]. So far, only angular distributions of the electron have been reported [51–53]. The fraction of the photon momentum given to the ion can be deducted from the angular distributions with momentum conservation arguments.

8.2. Multi-photon ionization and strong-field ionization

The question on how the photon linear momentum was shared between the electron and the ion in strong-field or multi-photon ionization was addressed in reference [11]. The authors concluded from their experimental data that the fraction of I_p/c is transferred to the ion whereas the fraction E_{kin}/c is transferred to the electron. In addition, the authors concluded that the additional energy U_p/c that is necessary to lift the electron into the continuum does not transfer any net linear momentum to the photoelectron. It should be noted that the authors drew their conclusions from photoelectron distributions alone and no measurement of the ion momentum was done. In addition, the error bars were rather large given the small magnitude of the actually measured shifts.

Calculations have shown that there are deviations from this momentum sharing for 1s-state of atomic hydrogen around $\frac{I_p}{3c}$ [74, 76, 98]. The result was confirmed for an initial s-state [12, 68].

The deviation of $\frac{I_p}{3c}$ was observed in a recent experiment [36] for circular polarization. The shift was observed as an offset to the energy-dependent shift along the beam-propagation direction for strong-field ionization of argon in circularly polarized 25 fs laser pulses with a centre wavelength of 800 nm. However, this deviation could not be observed with linear polarization [36].

According to predictions from theory, the deviation appears to differ significantly from $\frac{I_p}{3c}$ for an the initial state other than an s-state [77]. SFA-calculations predict deviations ranging from $-0.9\frac{I_p}{c}$ to $0.6\frac{I_p}{c}$ for different $n = 2$ angular momentum states. The latter result has not yet been observed experimentally.

In conclusion, so far there has been only a few experiments for the momentum sharing between the electron and the ion in strong-field physics. In particular no experiments have been reported so far that measure the momenta of the electron and the ion in coincidence. Such experiments would

shed some more light on the momentum sharing between the photofragments.

9. Future directions

9.1. Momentum sharing between the ion and the electron

9.1.1. Single-photon ionization. Until very recently [47], there have been no systematic experimental studies on the momentum sharing between the electron and the ion where both the final momentum of the photoelectron and the parent ion were measured in coincidence. The results from reference [47] mark the first measurement of the photoelectron as well as the ion to obtain reliable information about the momentum sharing between the photoelectron and the ion. The results of reference [47] represent the result of an initial 1s-state and pave the way to further studies on different angular momentum and energy state states. Theory predicts different momentum sharing for different initial angular momentum states [112, 115]. So far, the influence of the initial state onto the final momentum sharing has never been studied experimentally with measurements on both the electrons and the ions despite its fundamental nature and its importance for a variety of fields such as for example astrophysics. The measurements could also be extended to molecules, including fragmentation processes.

9.1.2. Multi-photon and strong-field ionization. To date all measurements on non-dipole effects in the multi-photon and the strong-field regime focussed on the photoelectrons. Therefore conclusions on the momentum sharing have been deducted from measurements of the photoelectron momentum and momentum conservation arguments. A measurement of the electron and the ion in the non-dipole regime has not yet been reported, at least not with sufficient resolution and accuracy to reliably conclude on the momentum sharing. Such measurements would be particularly interesting with sub-cycle time resolution such as in reference [8].

As in single photon ionization, the fraction of the momentum that is transferred to the photoelectron depends on the initial state, at least according to recently published SFA-calculations [77]. To date this subject has not been studied experimentally.

9.2. Attosecond time resolution of the photon momentum transfer

To date the only measurement with an attosecond time resolution of the linear multi-photon momentum transfer was performed in the strong-field field regime with the attoclock method [8] on xenon. The study motivates further studies with targets with various ionization potential and different wavelengths and intensities.

The attosecond time dependence of the linear photon momentum transfer in the case of single photon ionization would be highly interesting due to its fundamental nature. So far, measurements of the time delay in single photon ionization have been reported with the RABBITT and the streaking methods. The measurements focussed on the timing of the transfer

of the kinetic energy from the photon to the electron wave packet [116–122]. Similar to strong-field ionization it would be interesting to measure both the time- and energy-dependent p_z-shift of the photoelectron along the beam propagation direction. This could for example address the question if the energy and the linear momentum are transferred simultaneously to the electron or if time delays occur, as observed in the case of strong-field ionization. First predictions about a possible influence of the linear photon momentum on such measurements were reported in reference [12].

10. Concluding remarks

In this review, we summarized the recent results and showed not only the important effects beyond the dipole approximation, but we also demonstrated its potential to obtain additional information about fundamental processes in light–matter interaction. We put our research results in a broader context with additional discussions about other efforts and the connection to measurements of single photon ionization.

Ever since our initial publication of reference [5] in 2014 there has been an increasing number of new observations of non-dipole effects, leading to the fact that during the preparation of this review we even had trouble to keep up with the new publications on this topic.

Despite of all these new articles the exploration has not yet saturated. We have suggested more exciting experiments and discussed still open issues that need to be resolved. In particular, time-dependent measurements have the potential to provide deeper insight into fundamental mechanisms that is not only restricted to single ionization but can also be extended to multi ionization processes.

The emergence of novel light sources operating at high intensities and long wavelengths will enable more exciting experiments in this field.

We hope that with this review we can make the atomic, molecular and optical science community more aware of the effects beyond the dipole approximation and in particular its fundamental implications and possible applications.

Data availability statement

No new data were created or analysed in this study.

Appendix A. Atomic units and SI-units

Throughout the article, we use atomic units, unless stated otherwise. Atomic units are defined by the relations

$$\hbar = m_e = e^2 = 1. \tag{28}$$

The occasion when SI-units are used are mainly for the intensity and the wavelength. We present in this appendix briefly the conversion relation between atomic units and SI units. More comprehensive overviews on atomic unit systems and their conversion to other unit systems can be found for example in reference [123].

A.1. Length, time, velocity and momentum

The unit of length in atomic units is the Bohr radius a_0, i.e. the most probable distance of an electron from the centre of the nucleus in a hydrogen atom in the ground state:

$$r[\text{a.u.}] = \frac{r[\text{m}]}{5.291\,772\,49 \cdot 10^{-11}\ \text{m}}. \tag{29}$$

In analogy, the velocity in atomic units corresponds to the velocity of an electron in the first Bohr orbit:

$$v[\text{a.u.}] = \frac{v\left[\text{m s}^{-1}\right]}{2.187\,691\,42 \cdot 10^6\ \text{m s}^{-1}} \tag{30}$$

The velocity can be converted to the momentum of an electron in the first Bohr orbit by the multiplication with the electron mass, resulting in the atomic unit for the momentum:

$$p[\text{a.u.}] = \frac{p\left[\text{kg} \cdot \text{m s}^{-1}\right]}{1.992\,851\,91 \cdot 10^{-24}\ \text{kg} \cdot \text{ms}^{-1}} \tag{31}$$

The atomic unit of time is in turn the time that electron with the velocity of 1 a.u. needs to travel the distance of 1 atomic unit:

$$t[\text{a.u.}] = \frac{t[\text{s}]}{2.418\,884\,33 \cdot 10^{-17}\ \text{s}}. \tag{32}$$

A.2. Energy and frequency

The atomic unit of energy (also called Hartree) is the potential energy (i.e. twice the binding energy) of an electron in the ground state of a hydrogen atom:

$$E[\text{a.u.}] = \frac{E[\text{eV}]}{27.211\ \text{eV}} = \frac{E[\text{J}]}{4.359\,744\,72 \cdot 10^{-18}\ \text{J}}. \tag{33}$$

The atomic unit of frequency is the inverse of the atomic unit of time:

$$\nu[\text{a.u.}] = \frac{\nu[\text{Hz}]}{4.134\,137\,32 \cdot 10^{16}\ \text{Hz}}. \tag{34}$$

The atomic unit for the angular frequency is obtained by the multiplication of the frequency with 2π and is in atomic units, due to $\hbar = 1$, equal to the energy.

A.3. Intensity and electric field

The atomic unit of the electric field strength that an electron in the first Bohr radius experiences and is deducted from the ratio of the atomic unit of energy and length. The electric field in atomic units relates to the electric field in SI-units via

$$E[\text{a.u.}] = \frac{E\left[\text{V m}^{-1}\right]}{5.142\,208\,26 \cdot 10^{11}\ \text{V m}^{-1}} \tag{35}$$

A light field with an electric field strength $\frac{E_0}{\sqrt{1+\epsilon^2}}$, where ϵ denotes the ellipticity, has in atomic units the intensity $I = E_0^2$.

The intensity in atomic units and SI-units are related as follows:

$$I[\text{a.u.}] = \frac{I[\text{W cm}^{-2}]}{3.509\,447\,58 \cdot 10^{16}\ \text{W cm}^{-2}}. \tag{36}$$

ORCID iDs

J Maurer ⓘ https://orcid.org/0000-0001-8003-1015
U Keller ⓘ https://orcid.org/0000-0002-1689-8041

References

[1] Schiff L 1955 *Quantum Mechanics* (*International Series in Pure and Applied Physics*) (New York: McGraw-Hill)
[2] Milosevic N, Corkum P B and Brabec T 2004 *Phys. Rev. Lett.* **92** 013002
[3] Moore C I, Knauer J P and Meyerhofer D D 1995 *Phys. Rev. Lett.* **74** 2439
[4] Meyerhofer D D, Knauer J P, McNaught S J and Moore C I 1996 *J. Opt. Soc. Am.* B **13** 113–7
[5] Ludwig A, Maurer J, Mayer B W, Phillips C R, Gallmann L and Keller U 2014 *Phys. Rev. Lett.* **113** 243001
[6] Reiss H R 2008 *Phys. Rev. Lett.* **101** 043002
[7] Maurer J *et al* 2018 *Phys. Rev.* A **97** 013404
[8] Willenberg B, Maurer J, Mayer B W and Keller U 2019 *Nat. comm.* **10** 1–8
[9] Daněk J, Hatsagortsyan K Z and Keitel C H 2018 *Phys. Rev.* A **97** 063409
[10] Willenberg B, Maurer J, Keller U, Daněk J, Klaiber M, Teeny N, Hatsagortsyan K Z and Keitel C H 2019 *Phys. Rev.* A **100** 033417
[11] Smeenk C T L, Arissian L, Zhou B, Mysyrowicz A, Villeneuve D M, Staudte A and Corkum P B 2011 *Phys. Rev. Lett.* **106** 193002
[12] Jensen S V B, Lund M M and Madsen L B 2020 *Phys. Rev.* A **101** 043408
[13] Wang M-X, Chen S-G, Liang H and Peng L-Y 2020 *Chin. Phys.* B **29** 013302
[14] Haram N, Sang R T and Litvinyuk I V 2020 *J. Phys. B: At. Mol. Opt. Phys.* **53** 154005
[15] Di Piazza A, Müller C, Hatsagortsyan K Z and Keitel C H 2012 *Rev. Mod. Phys.* **84** 1177
[16] Landau L D and Lifshitz E M 1975 *The Classical Theory of Fields* (Amsterdam: Elsevier)
[17] Kobe D H 1982 *Am. J. Phys.* **50** 128–33
[18] Reiss H R 1992 *Prog. Quantum Electron.* **16** 1–71
[19] Göppert-Mayer M 1931 *Ann. Phys.* **401** 273–94
[20] Reiss H 2013 *Phys. Rev.* A **87** 033421
[21] Reiss H R 2014 *J. Phys. B: At. Mol. Opt. Phys.* **47** 204006
[22] Kylstra N J, Potvliege R M and Joachain C J 2001 *J. Phys. B: At. Mol. Opt. Phys.* **34** L55
[23] Simonsen A S and Førre M 2016 *Phys. Rev.* A **93** 063425
[24] Førre M and Simonsen A S 2016 *Phys. Rev.* A **93** 013423
[25] Volkow D M 1935 *Z. Phys.* **94** 250–60 250
[26] van Linden van den Heuvell H B and Muller H G 1987 *Multiphoton Processes* (Cambridge: Cambridge University Press)
[27] Corkum P B 1993 *Phys. Rev. Lett.* **71** 1994
[28] Sarachik E S and Schappert G T 1970 *Phys. Rev.* D **1** 2738–53
[29] Kylstra N J, Worthington R A, Patel A, Knight P L, Vázquez de Aldana J R and Roso L 2000 *Phys. Rev. Lett.* **85** 1835

[30] Joachain C J, Kylstra N J and Potvliege R M 2012 *Atoms in Intense Laser Fields* (Cambridge: Cambridge University Press)

[31] Palaniyappan S, Ghebregziabher I, DiChiara A D, MacDonald J and Walker B C 2006 *Phys. Rev. A* **74** 033403

[32] Klaiber M, Hatsagortsyan K Z, Wu J, Luo S S, Grugan P and Walker B C 2017 *Phys. Rev. Lett.* **118** 093001

[33] Daněk J *et al* 2018 *J. Phys. B: At. Mol. Opt. Phys.* **51** 114001

[34] Keldysh L V 1965 *Sov. Phys. JETP* **20** 1307–14

[35] Reiss H R 1990 *Phys. Rev. A* **42** 1476

[36] Hartung A *et al* 2019 *Nat. Phys.* **15** 1222–6

[37] Eppink A T J B and Parker D H 1997 *Rev. Sci. Instrum.* **68** 3477–84

[38] Parker D H and Eppink A T J B 1997 *J. Chem. Phys.* **107** 2357–62

[39] Kling N G *et al* 2014 *J. Inst.* **9** P05005

[40] Wollenhaupt M, Lux C, Krug M and Baumert T 2013 *ChemPhysChem* **14** 1341–9

[41] Maurer J, Dimitrovski D, Christensen L, Madsen L B and Stapelfeldt H 2012 *Phys. Rev. Lett.* **109** 123001

[42] Smeenk C, Salvail J Z, Arissian L, Corkum P B, Hebeisen C T and Staudte A 2011 *Opt. Express* **19** 9336

[43] Dimitrovski D, Maurer J, Stapelfeldt H and Madsen L B 2014 *Phys. Rev. Lett.* **113** 103005

[44] Dörner R, Mergel V, Jagutzki O, Spielberger L, Ullrich J, Moshammer R and Schmidt-Böcking H 2000 *Phys. Rep.* **330** 95–192

[45] Ullrich J, Moshammer R, Dorn A, D rner R, Schmidt L P H and Schmidt-Böcking H 2003 *Rep. Prog. Phys.* **66** 1463

[46] Haram N *et al* 2019 *Phys. Rev. Lett.* **123** 093201

[47] Grundmann S *et al* 2020 *Phys. Rev. Lett.* **124** 233201

[48] Mayer B W, Phillips C R, Gallmann L, Fejer M M and Keller U 2013 *Opt. Lett.* **38** 4265–8

[49] Mayer B W, Phillips C R, Gallmann L and Keller U 2014 *Opt. Express* **22** 20798–808

[50] Pupeikis J, Chevreuil P-A, Bigler N, Gallmann L, Phillips C R and Keller U 2020 *Optica* **7** 168–71

[51] Cooper J W 1993 *Phys. Rev. A* **47** 1841–51

[52] Krässig B, Jung M, Gemmell D S, Kanter E P, LeBrun T, Southworth S H and Young L 1995 *Phys. Rev. Lett.* **75** 4736–9

[53] Hemmers O *et al* 1997 *J. Phys. B: At. Mol. Opt. Phys.* **30** L727–33

[54] Bardsley J N, Penetrante B M and Mittleman M H 1989 *Phys. Rev. A* **40** 3823–35

[55] Ammosov M V, Delone N B and Krainov V P 1986 *Zh. Eksp. Teor. Fiz.* **91** 2008

[56] Perelomov A M and Popov V S 1967 *Zh. Exp. Theor. Fiz.* **52** 514–26

[57] Goreslavski S P, Paulus G G, Popruzhenko S V and Shvetsov-Shilovski N I 2004 *Phys. Rev. Lett.* **93** 233002

[58] Perelomov A M and Popov V S 1966 *Zh. Exp. Theor. Fiz.* **50** 1393–409

[59] Perelomov A M, Popov V S and Terent'ev V M 1966 *Zh. Exp. Theor. Fiz.* **51** 309–26

[60] Popov V S, Kuznetsov V P and Perelomov A M 1967 *Zh. Exp. Theor. Fiz* 331

[61] Mur V D, Popruzhenko S V and Popov V S 2001 *Zh. Exp. Theor. Fiz.* **119** 893–905

[62] Popov V S 1999 *Phys.-Usp.* **42** 733–4

[63] Popov V S 2004 *Phys.-Usp.* **47** 855

[64] Barth I and Smirnova O 2014 *J. Phys. B: At. Mol. Opt. Phys.* **47** 204020

[65] Lai Y H *et al* 2017 *Phys. Rev. A* **96** 063417

[66] Fu L B, Liu J, Chen J and Chen S G 2001 *Phys. Rev. A* **63** 043416

[67] Pfeiffer A N, Cirelli C, Smolarski M, Dimitrovski D, Abu-samha M, Madsen L B and Keller U 2012 *Nat. Phys.* **8** 76

[68] Ni H *et al* 2020 *Phys. Rev. Lett.* **125** 073202

[69] Klaiber M, Yakaboylu E, Bauke H, Hatsagortsyan K Z and Keitel C H 2013 *Phys. Rev. Lett.* **110** 153004

[70] Popov V S, Karnakov B M, Mur V D and Pozdnyakov S G 2006 *J. Exp. Theor. Phys.* **102** 760

[71] Li M, Geng J W, Liu H, Deng Y, Wu C, Peng L Y, Gong Q and Liu Y 2014 *Phys. Rev. Lett.* **112** 113002

[72] Faisal F H M 1973 *J. Phys. B: At. Mol. Opt. Phys.* **6** L89

[73] Reiss H R 1980 *Phys. Rev. A* **22** 1786

[74] Klaiber M, Hatsagortsyan K Z and Keitel C H 2005 *Phys. Rev. A* **71** 033408

[75] Klaiber M, Yakaboylu E and Hatsagortsyan K Z 2013 *Phys. Rev. A* **87** 023417

[76] Chelkowski S, Bandrauk A D and Corkum P B 2014 *Phys. Rev. Lett.* **113** 263005

[77] He P L, Lao D and He F 2017 *Phys. Rev. Lett.* **118** 163203

[78] Titi A S and Drake G W F 2012 *Phys. Rev. A* **85** 041404

[79] Huismans Y *et al* 2011 *Science* **331** 61–4

[80] Keil T and Bauer D 2017 *J. Phys. B: At. Mol. Opt. Phys.* **50** 194002

[81] Bugacov A, Pont M and Shakeshaft R 1993 *Phys. Rev. A* **48** R4027

[82] de Aldana J V and Roso L 1999 *Opt. Express* **5** 144–8

[83] de Aldana J V, Kylstra N, Roso L, Knight P, Patel A and Worthington R 2001 *Phys. Rev. A* **64** 013411

[84] Meharg K J, Parker J S and Taylor K T 2005 *J. Phys. B: At. Mol. Opt. Phys.* **38** 237

[85] Brennecke S and Lein M 2018 *J. Phys. B: At. Mol. Opt. Phys.* **51** 094005

[86] Brennecke S and Lein M 2018 *Phys. Rev. A* **98** 063414

[87] Chelkowski S, Bandrauk A D and Corkum P B 2015 *Phys. Rev. A* **92** 051401

[88] Guo D S and Aberg T 1988 *J. Phys. A: Math. Gen.* **21** 4577–91

[89] Guo D-S and Drake G W F 1992 *Phys. Rev. A* **45** 6622–35

[90] Agostini P, Fabre F, Mainfray G, Petite G and Rahman N K 1979 *Phys. Rev. Lett.* **42** 1127–30

[91] Eckle P, Smolarski M, Schlup P, Biegert J, Staudte A, Schöffler M, Muller H G, Dörner R and Keller U 2008 *Nat. Phys.* **4** 565

[92] Eckle P, Pfeiffer A N, Cirelli C, Staudte A, Dörner R, Muller H G, Büttiker M and Keller U 2008 *Science* **322** 1525

[93] Hofmann C, Landsman A S and Keller U 2019 *J. Mod. Opt.* **66** 1052–70

[94] Førre M, Hansen J, Kocbach L, Selstø S and Madsen L B 2006 *Phys. Rev. Lett.* **97** 043601

[95] Førre M, Selstø S, Hansen J P, Kjeldsen T K and Madsen L B 2007 *Phys. Rev. A* **76** 033415

[96] Tao J, Xia Q, Cai J, Fu L and Liu J 2017 *Phys. Rev. A* **95** 011402

[97] Spanner M, Smirnova O, Corkum P B and Ivanov M Y 2004 *J. Phys. B: At. Mol. Opt. Phys.* **37** L243

[98] Chelkowski S, Bandrauk A D and Corkum P B 2017 *Phys. Rev. A* **95** 053402

[99] Brennecke S and Lein M 2019 *Phys. Rev. A* **100** 023413

[100] Figueira de Morisson Faria C, Schomerus H, Liu X and Becker W 2004 *Phys. Rev. A* **69** 043405

[101] Weber T *et al* 2000 *Nature* **405** 658–61

[102] Pfeiffer A N, Cirelli C, Smolarski M, Dörner R and Keller U 2011 *Nat. Phys.* **7** 428–33

[103] Pfeiffer A N, Cirelli C, Smolarski M, Wang X, Eberly J H, Dörner R and Keller U 2011 *New J. Phys.* **13** 093008

[104] Sun F *et al* 2020 *Phys. Rev. A* **101** 021402

[105] Emmanouilidou A and Meltzer T 2017 *Phys. Rev. A* **95** 033405

[106] Chen X, Ruiz C, He F and Zhang J 2020 *Opt. Express* **28** 14884–96

[107] Zhu X and Wang Z 2016 *Opt. Commun.* **365** 125–32
[108] Walser M W, Keitel C H, Scrinzi A and Brabec T 2000 *Phys. Rev. Lett.* **85** 5082–5
[109] Pisanty E, Hickstein D D, Galloway B R, Durfee C G, Kapteyn H C, Murnane M M and Ivanov M 2018 *New J. Phys.* **20** 053036
[110] Mishra R, Kalita D and Gupta A 2012 *Eur. Phys. J.* D **66** 1–5
[111] Bandrauk A and Lu H 2006 *Phys. Rev.* A **73** 013412
[112] Sommerfeld A and Schur G 1930 *Ann. Phys.* **396** 409–32
[113] Michaud G 1970 *Astrophys. J.* **160** 641
[114] Seaton M J 1995 *J. Phys. B: At. Mol. Opt. Phys.* **28** 3185
[115] Massacrier G 1996 *Astron. Astrophys.* **309** 979–90
[116] Schultze M *et al* 2010 *Science* **328** 1658–62
[117] Klünder K *et al* 2011 *Phys. Rev. Lett.* **106** 143002

[118] Nagele S, Pazourek R, Feist J, Doblhoff-Dier K, Lemell C, Tökési K and Burgdörfer J 2011 *J. Phys. B: At. Mol. Opt. Phys.* **44** 081001
[119] Dahlström J M, Guénot D, Klünder K, Gisselbrecht M, Mauritsson J, L'Huillier A, Maquet A and Taïeb R 2013 *Chem. Phys.* **414** 53–64
[120] Pazourek R, Nagele S and Burgdörfer J 2015 *Rev. Mod. Phys.* **87** 765
[121] Sabbar M, Heuser S, Boge R, Lucchini M, Carette T, Lindroth E, Gallmann L, Cirelli C and Keller U 2015 *Phys. Rev. Lett.* **115** 133001
[122] Vos J, Cattaneo L, Patchkovskii S, Zimmermann T, Cirelli C, Lucchini M, Kheifets A, Landsman A S and Keller U 2018 *Science* **360** 1326–30
[123] Krainov V P, Reiss H R and Smirnov B M 1997 *Radiative Processes in Atomic Physics* (New York: Wiley)